Uncommon quadruple stacking topology in a honeycomb-sheet MOF compatible with through-space conduction

Tappei Tanabe,[a,b] Liyuan Qu,[b] Kenta Ueno,[a] Shinya Takaishi,[a] Masahiro Yamashita,[a,c] Yuh Hijikata,[d] Ryotaro Matsuda,[b] Ryota Sakamoto[a] and Hiroaki Iguchi*[b]

a. Department of Chemistry, Graduate School of Science, Tohoku University, 6-3 Aramaki-Aza-Aoba, Aoba-ku, Sendai, Miyagi 980-8578, Japan.
b. Department of Materials Chemistry, Graduate School of Engineering, Nagoya University, Chikusa-ku, Nagoya 464-8603, Japan
c. School of Chemical Science and Engineering, Tongji University, Shanghai 559 200092, P.R. China
d. Research Center for Net Zero Carbon Society, Institutes of Innovation for Future Society, Nagoya University, Chikusa-ku, Nagoya 464-8601, Japan

Table of Contents

Experimental details

General experimental information

All chemicals were used without further purification. IR spectra were collected with KBr pellets on a JASCO FT/IR-4200 spectrometer at room temperature (RT). UV-Vis-NIR absorption spectra were collected with KBr pellets on a JASCO V-670 spectrophotometer at RT. KBr pellets were prepared in a glovebox (MBRAUN UNILAB1200/780) filled with Ar gas, and then sealed in a custom cell for IR and UV-Vis-NIR measurement under an inert atmosphere. Thermogravimetry analysis (TGA) was carried out on a SHIMADZU DTG-60H with a heating rate of 5 °C/min under a constant nitrogen gas flow (0.1 L/min). Powder X-ray diffraction (PXRD) patterns were collected on a Bruker SmartLab with Cu Kα radiation (λ = 1.5406 Å) at RT. Samples were prepared in a glovebox filled with Ar gas, and then sealed in a capillary. ^{1}H NMR measurements were performed on Bruker AV500 at RT. The temperature dependence of the electrical conductivity was measured in a liquid He cryostat of a Quantum Design Physical Property Measuring System (PPMS) MODEL 6000 by using the two-probe method in direct current (DC) mode with Keithley sourcemeter model 2611. The cooling rate was 1K/min. The electrical leads (15 μmφ gold wires) were attached to a single crystal with carbon paste (Dotite XC-12 in diethyl succinate).

Single-crystal X-ray structure determination

The diffraction data for **PMC-20** were collected on a diffractometer equipped with a beamline BL-17A at Photon Factory in High Energy Accelerator Research Organization (KEK) with a Dectris Eiger X16M detector (synchrotron, λ = 0.900 Å, T = 120 K). XDS software was used for the processing and data reduction.[S1] The crystal structure was solved using direct methods (SHELXT[S2]) followed by Fourier synthesis. Structure refinement was performed using full-matrix least-squares procedures with SHELXL[S3] on F^2, where F is the crystal structure factor, in the Olex2 software.[S4] All non-hydrogen atoms were refined with anisotropic displacement parameters, while hydrogen atoms bonded to carbon were placed at geometrically calculated positions and refined with isotropic thermal parameters. Solvent mask was calculated with Olex2 to reduce the effect of residual electron densities of the highly disordered solvent molecules. 182 electrons were found in a volume of 530 Å^3 in a void per formula unit. This is almost consistent with the presence of two DMA (C_4H_9NO), two H_2O and one NMP (C_5H_9NO) molecules (162 electrons). (Note: the contribution of one oxygen atom of a solvent molecule coordinating to the Cd ion is not included in the mask.) Graphical material was prepared using Mercury CSD 4.2 software (copyright CCDC, https://www.ccdc.cam.ac.uk/mercury/).[S5]

Computational methods

The Amsterdam Density Functional (ADF) package, software based on density functional theory (DFT), in the Amsterdam Modeling Suite (AMS) packages[S6,S7] was applied for the calculations of transfer integral of **PMC-20**. The transfer integral between adjacent NDI-py molecules was investigated by the B3LYP-D3/TZP functional and basis set[S8] without structural optimization.

Syntheses

Synthesis of *N,N'*-bis(4-pyridyl)-naphthalenediimide (NDI-py)

Naphthalene-1,4,5,8-tetracarboxylic dianhydride 3.2 g (0.012 mol) and 4-aminopyridine 2.5 g (0.026 mol) in 20 mL *N,N*-dimetylformamide (DMF) were stirred at 180 ˚C overnight. After cooled to RT, precipitated solid was filtered and recrystallized by DMF. Pale brown crystals were washed by MeOH carefully, then dried in desiccator (1.45 g, 28.6%). ^{1}H NMR (500 MHz, DMSO-d_6, TMS) δ: 8.80–8.84 (dd, 4H), 8.74–8.78 (s, 4H), 7.57–7.60 (dd, 4H). Anal. Calc. for $C_{24}H_{12}N_4O_4$: C, 68.57; H, 2.88; N, 13.33. Found: C, 68.43; H, 2.96; N, 13.43

Synthesis of $[Cd(NDI\text{-}py)_{1.5}Br_{0.56}(OH_2)_{1.44}]\cdot NMP\cdot 2DMA\cdot 2H_2O$ **(PMC-20)**

PMC-20 was synthesized by liquid-liquid diffusion method in a glovebox filled with Ar gas. 1 mL DMA solution containing 4.1 mg (11.9 μmol) of $CdBr_2$ was slowly layered on 1 mL NMP solution containing 2.6 mg (6.1 μmol) of NDI-py and 1.6 mg (8.4 μmol) of cobaltocene. After two weeks, black rod-like single crystals were obtained (2.1 mg, 31.3%). Anal. Calc. for $C_{49}H_{51.88}N_9O_{12.44}Br_{0.56}Cd$: C, 52.40; H, 4.66; N, 11.22; Br, 3.99. Found: C, 52.33; H, 5.07; N, 11.17; Br, 4.05.

Exchange of lattice solvent molecules in **PMC-20**

PMC-20 was soaked in 10 mL of each solvent (methanol and acetone) for one week inside a glovebox. The crystals were then filtered within the glovebox.

Crystallographic data of PMC-20

Table S1 Crystallographic details for **PMC-20**

Radiation type, wavelength	Synchrotron, 0.90 Å
Empirical formula	C49 H51.88 Br0.56 Cd N9 O12.44
Formula weight	1123.06 g/mol
Crystal system	Orthorhombic
Space group	*Fddd*
Crystal size	0.11 × 0.025 × 0.009 mm^3
Crystal colour	Dark brown
Crystal shape	Plate
Unit cell dimensions	a = 9.679(5) Å
	b = 36.891(6) Å
	c = 54.555(13) Å
Volume	V = 19480(11) $Å^3$
Temperature	120 K
Z	16
Density (calculated)	1.532 Mg/m^3
Absorption coefficient	1.831 mm^{-1}
R_1, $wR_2[I > 2\sigma(I)]$	0.1112, 0.3577
R_1, wR_2[all data]	0.1178, 0.3635
$F(000)$	9216
Goodness of fit on F^2	1.595

Structural details and solvent-accessible voids of PMC-20

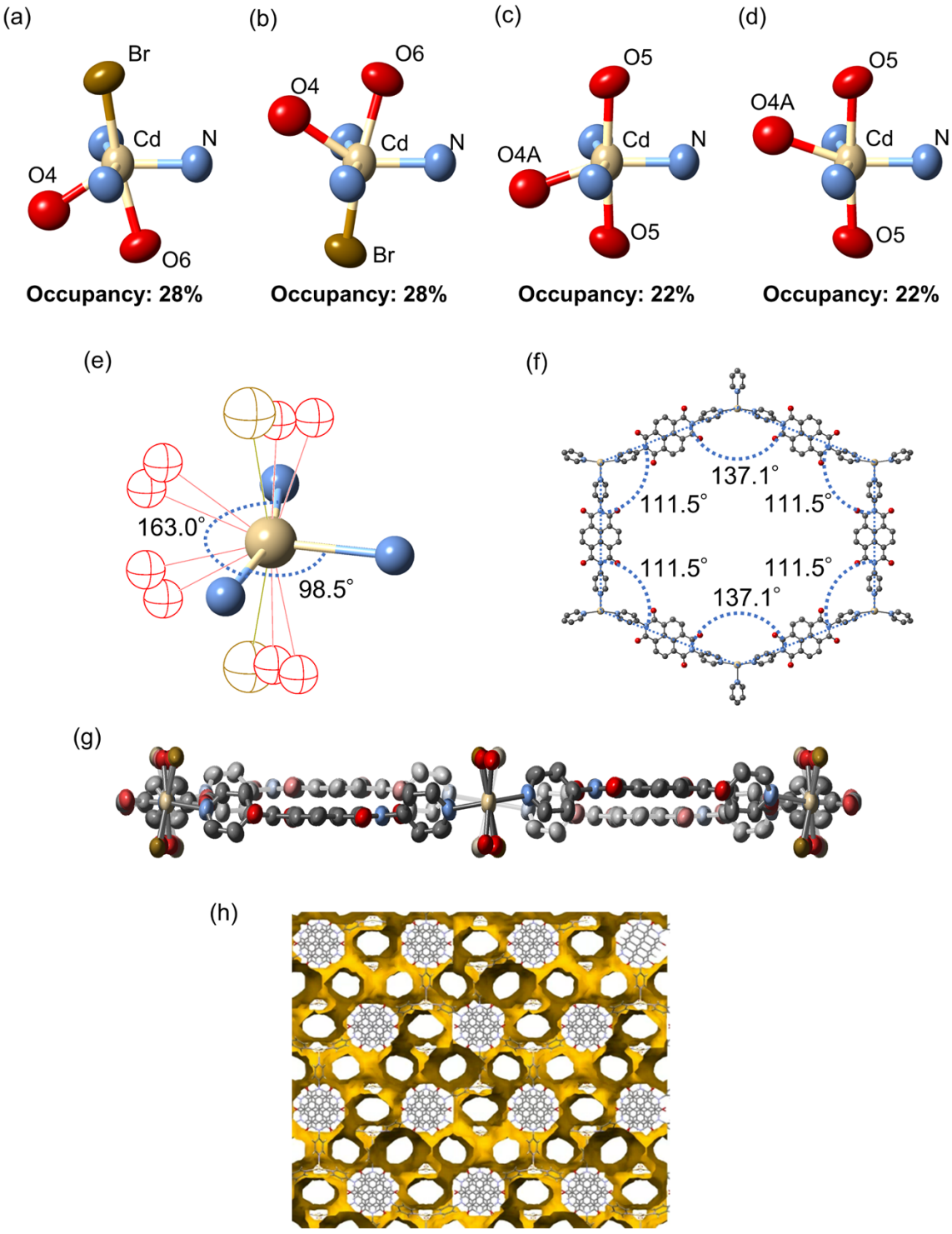

Fig. S1 Details of the crystal structure of **PMC-20**. (a−d) Four disordered coordination geometries around Cd^{2+} ion. (e) The N–Cd–N bond angles of *cis* and *trans* positions. (f) Angles of a hexagon in the honeycomb sheet. (g) Side view of the hexagon. (h) The solvent accessible voids of **PMC-20**. The contact surface of the voids (yellowish brown) is drawn by a probe radius of 1.4 Å. The void volume was calculated to be 42.4%.

ESR spectrum of PMC-20

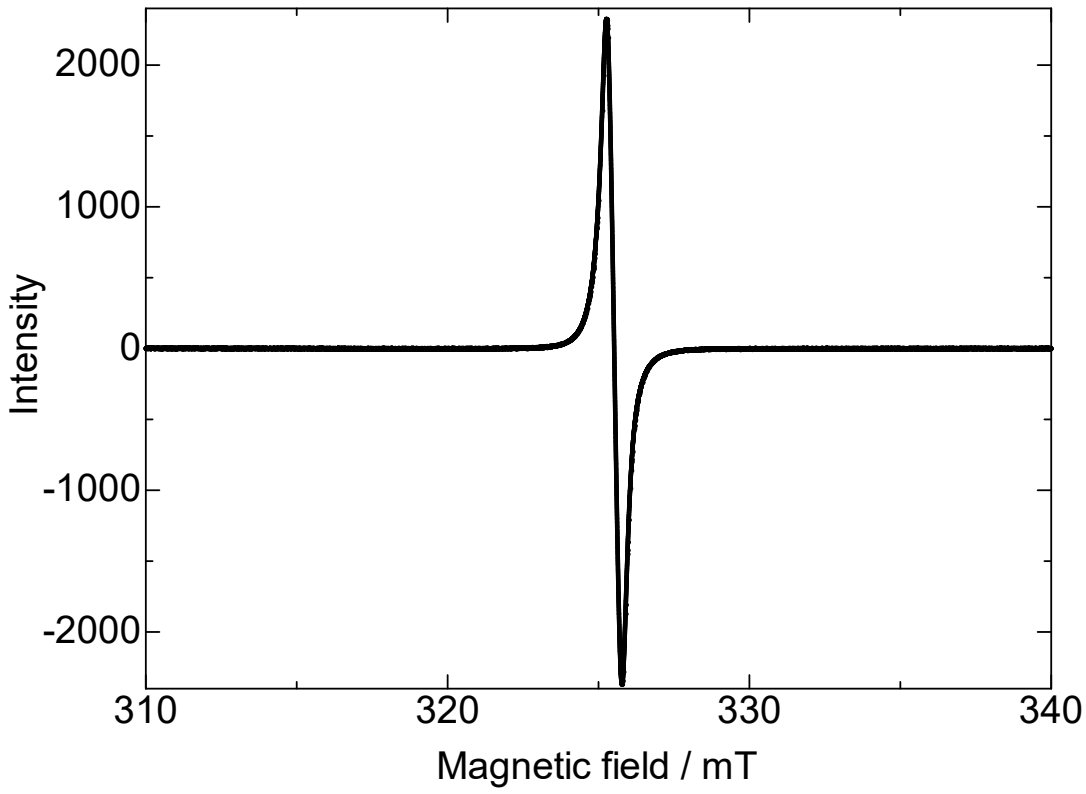

Fig. S2 Electron spin resonance (ESR) spectrum of **PMC-20** at room temperature

[1]H NMR spectrum of PMC-20

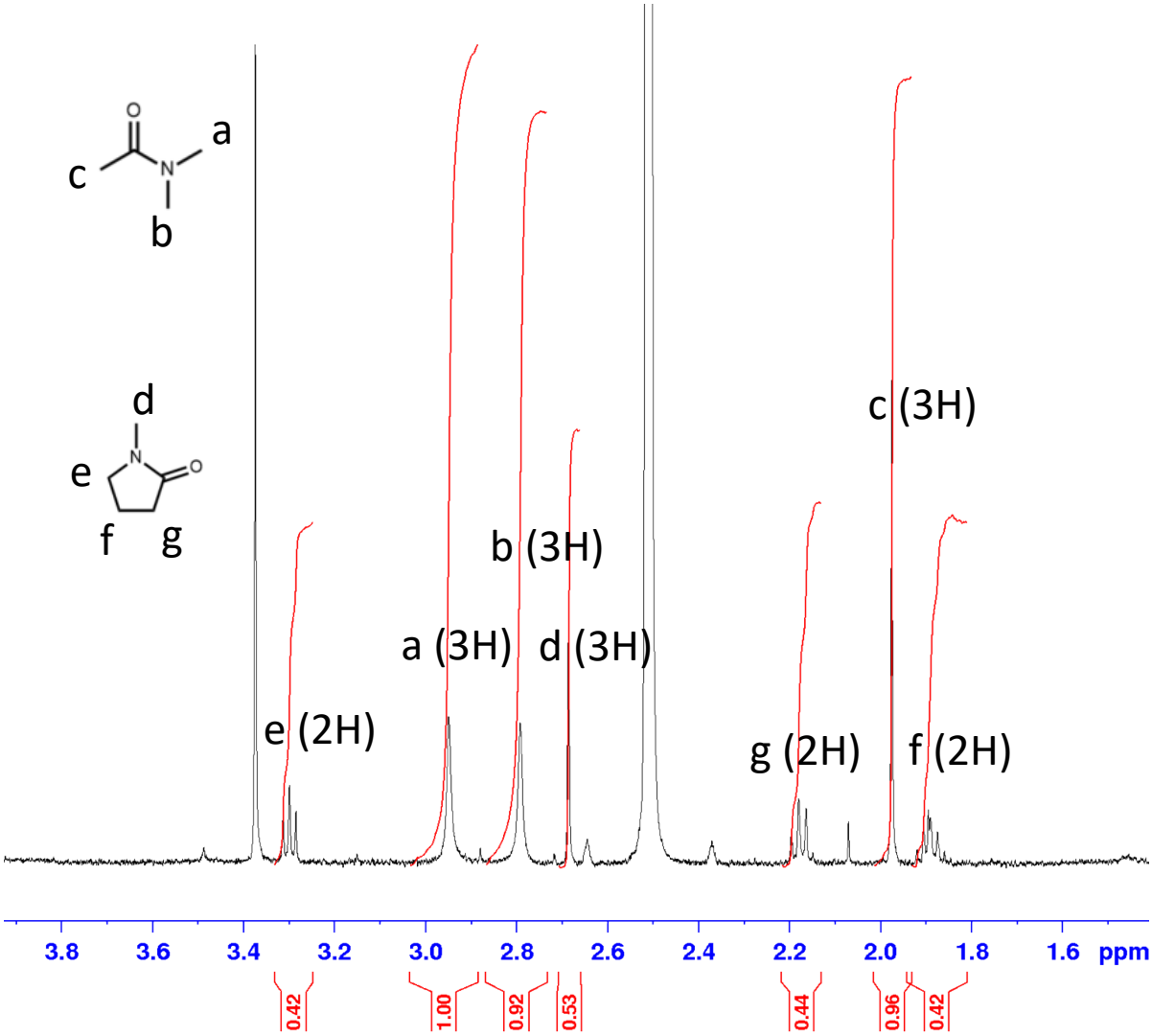

Fig. S3 [1]H NMR spectrum of **PMC-20** (500 MHz, DMSO-d_6, TMS)

To estimate the ratio of DMA to NMP molecules in the crystal, [1]H NMR spectrum of **PMC-20** was acquired at RT. A small drop of sulfuric acid was added to achieve perfect dissolution in DMSO-d_6.

On the basis of the integration values, the ratio of DMA to NMP was determined to be 1:2.

Thermogravimetric analyses (TGA) of PMC-20

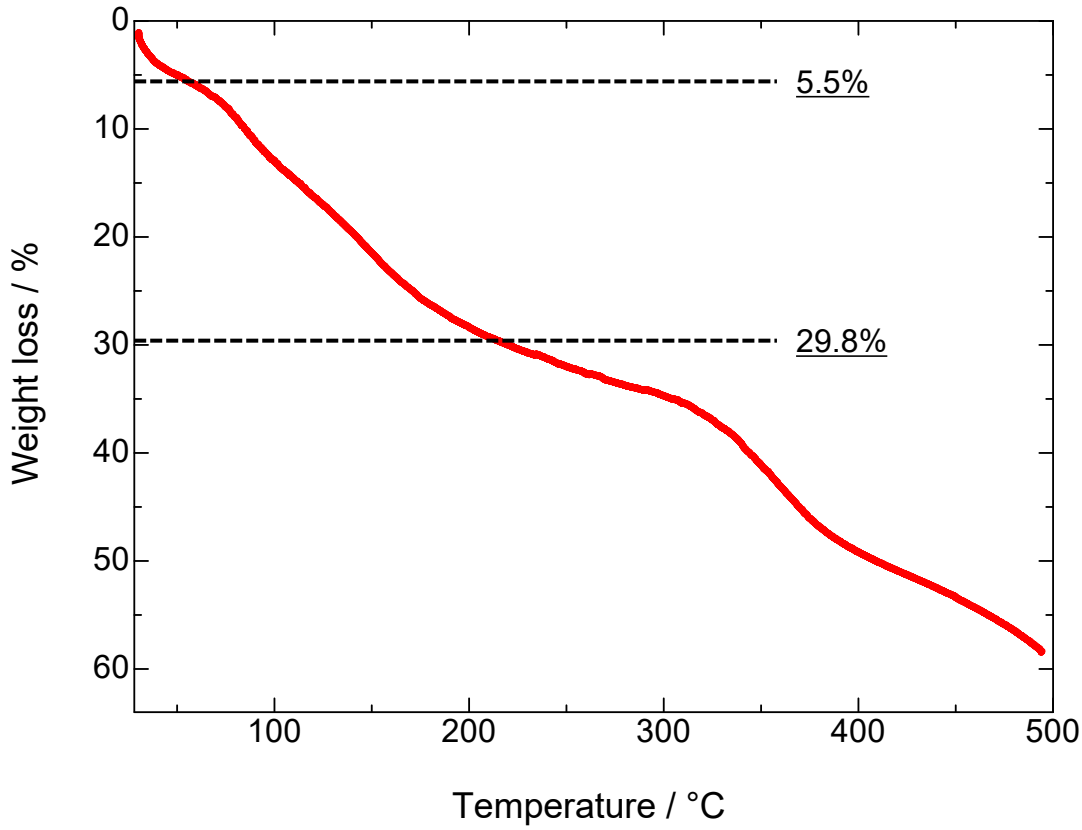

Fig. S4 Thermogravimetric analyses (TGA) of **PMC-20**

TGA indicated that there are two unclear steps of weight loss. The first weight loss up to 50°C corresponds to 3.44 water molecules (5.5%). The total weight of one NMP and two DMA molecules is calculated to be 24.3%, which should contribute to the second weight loss up to 200 °C. Further weight loss is probably due to the decomposition.

Variable-temperature powder X-ray diffraction (PXRD) patterns of PMC-20

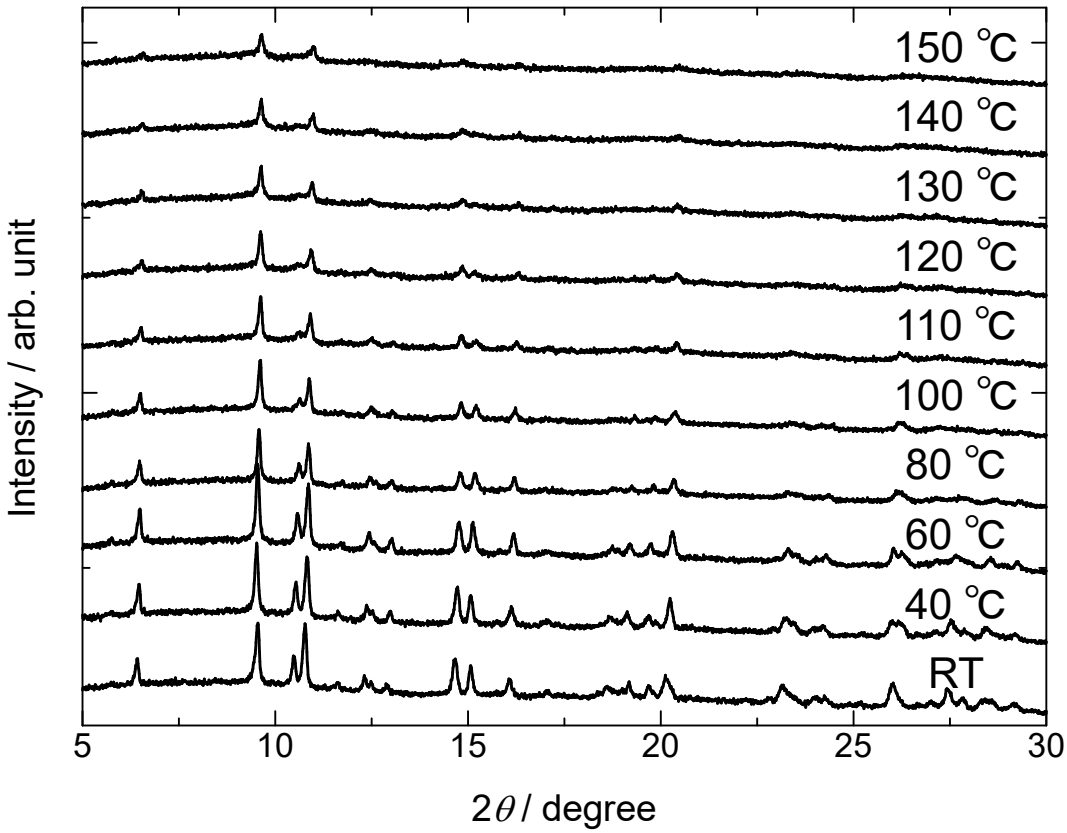

Fig. S5 Variable-temperature PXRD patterns of **PMC-20**

PXRD patterns of **PMC-20** were measured from RT to 150°C. There was no change in the PXRD pattern up to 60 °C, suggesting that the structural change does not occur under the liberation of H_2O. However, crystallinity became worse from 80 °C, and the patterns were almost disappeared at 150 °C. These results suggest that the structural change was caused by the loss of the coordinating NMP molecules and/or lattice DMA molecules.

^{1}H NMR spectra of PMC-20 after solvent exchange

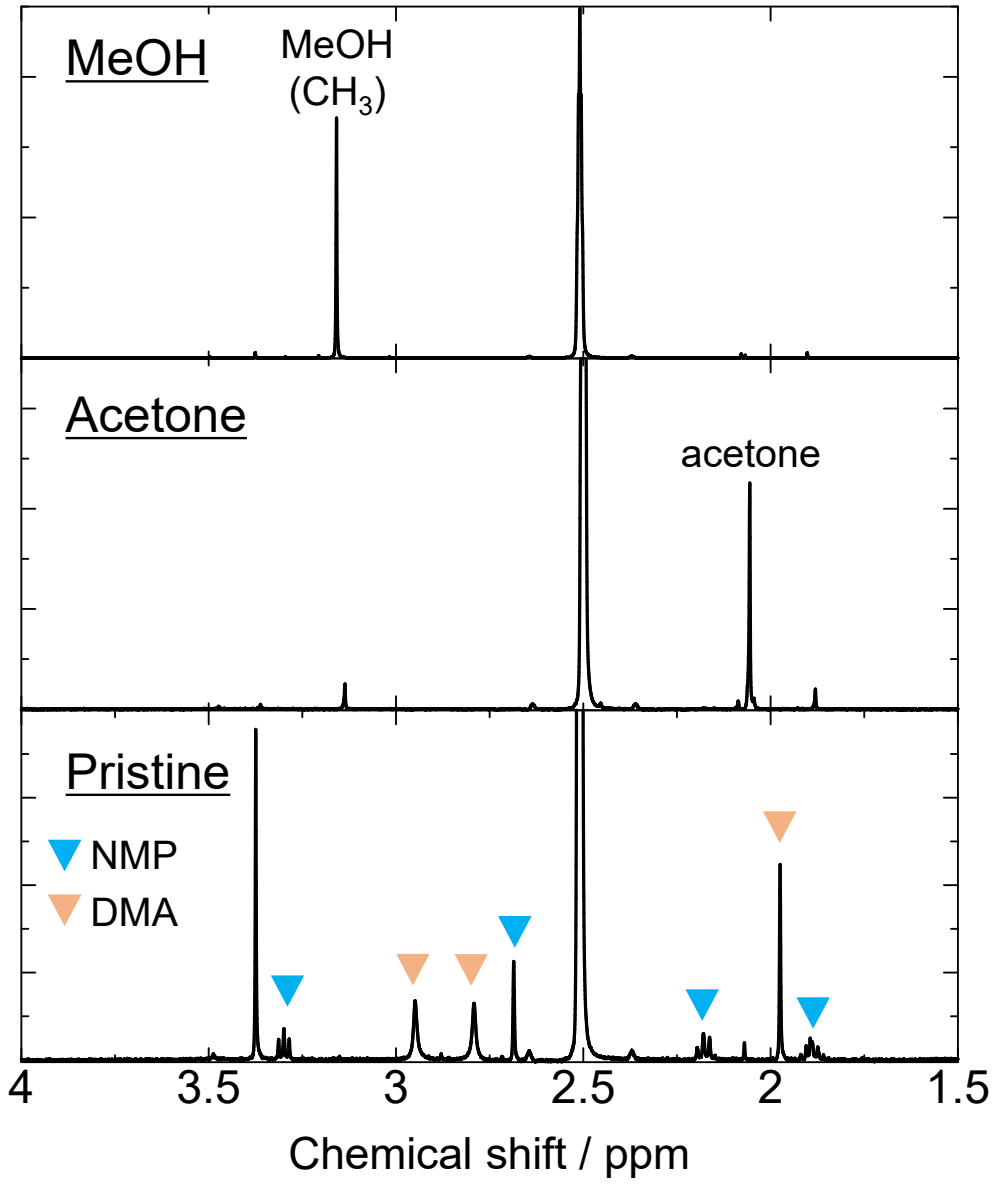

Fig. S6 ^{1}H NMR spectra of **PMC-20** after soaked in methanol and acetone with the spectrum pristine sample as a reference (500 MHz, DMSO-d_6, TMS)

^{1}H NMR spectra of **PMC-20** after soaking was acquired at RT. A small drop of sulfuric acid was added to achieve perfect dissolution in DMSO-d_6. Compared to the NMR spectrum of pristine **PMC-20**, the peaks assignable to DMA and NMP disappeared after soaking in MeOH or acetone. Instead, peaks corresponding to methanol (CH_3) and acetone appeared around 3.16 ppm and 2.06 ppm, respectively. These results indicate that the DMA and NMP molecules were replaced by the soaking solvent molecules.

Structural stability of PMC-20 under solvent exchange

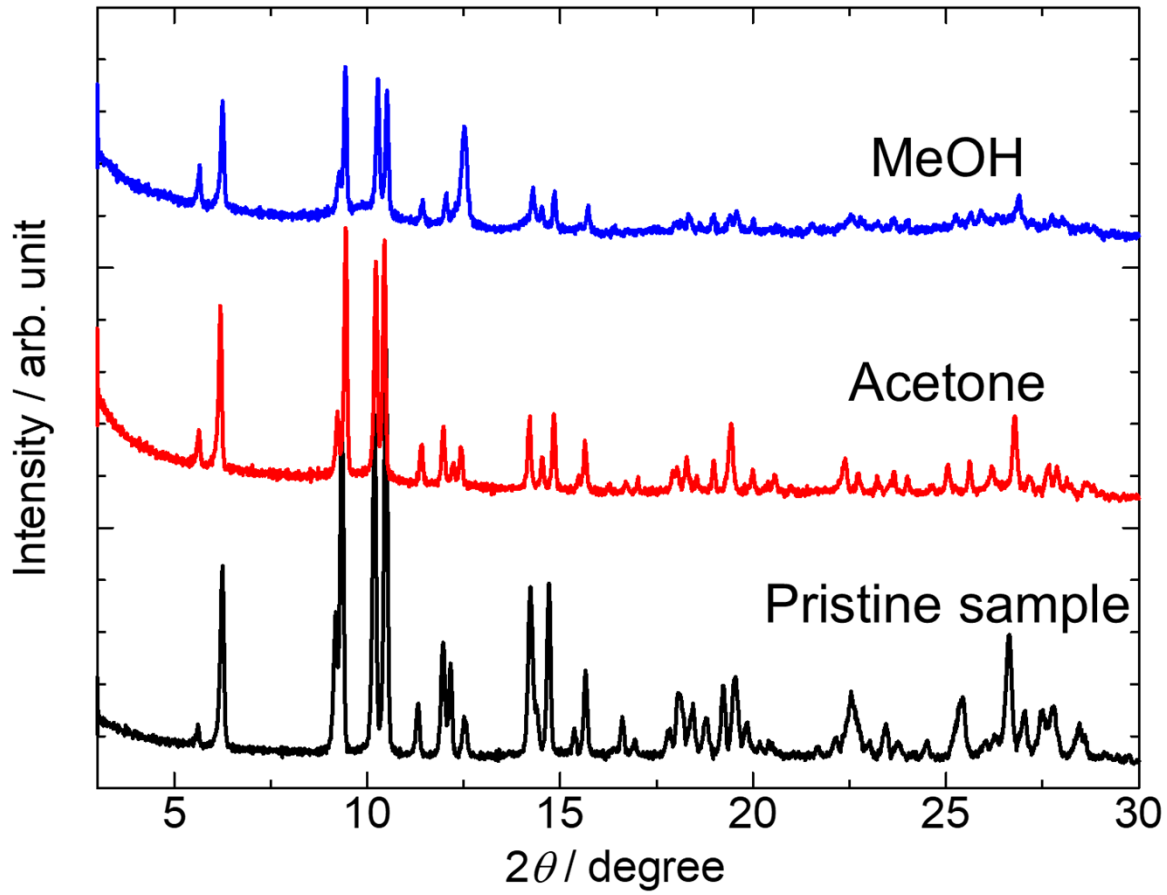

Fig. S7 Powder X-ray diffraction (PXRD) patterns of **PMC-20** after solvent exchange (black: pristine **PMC-20**, red: **PMC-20** soaked in acetone, blue: **PMC-20** soaked in methanol).

List of through-space conductive MOFs

Table S2 Selected electrically conductive MOFs with through-space conduction pathways

Material	σ_{RT}	Method	Reference
PMC-20	**7.6×10^{-3} S cm^{-1}**	**2-probe single crystal**	**This work**
PMC-1	3.3×10^{-3} S cm^{-1}	2-probe single crystal	S9
PMC-2	1.6×10^{-6} S cm^{-1}	2-probe single crystal	S10
PMC-hexagon	2.1×10^{-4} S cm^{-1}	2-probe pellet	S11
Cd_2(TTFTB)	2.9×10^{-4} S cm^{-1}	2-probe single crystal	S12
Mn_2(TTFTB)	9×10^{-5} S cm^{-1}	2-probe single crystal	S12
Zn_2(TTFTB)	4.0×10^{-6} S cm^{-1}	2-probe single crystal	S12
$Cd_{2.39}(TPDAP)_3$	1×10^{-6} S cm^{-1}	2-probe single crystal	S13
$ZnNa_2(AnBEB)_2$	1.3×10^{-3} S cm^{-1}	2-probe single crystal	S14
$La_{1.5}$(HOTP)	900 S cm^{-1}	4-probe single crystal	S15
$Nd_{1.5}$(HOTP)	1080 S cm^{-1}	4-probe single crystal	S15

References

[S1] W. Kabsch, *Acta Cryst.* **2010**, D*66*, 125–132.

[S2] G. M. Sheldrick, *Acta Cryst.*, **2015**, C*71*, 3–8.

[S3] G. M. Sheldrick, *Acta Cryst.,* **2015**, A*71*, 3–8.

[S4] O. V. Dolomanov, L. J. Bourhis, R. J. Gildea, J. A. K. Howard and H. Puschmann, *J. Appl. Cryst.*, **2009**, *42*, 339–341.

[S5] Mercury 4.0: from visualization to analysis, design and prediction
C. F. Macrae, I. Sovago, S. J. Cottrell, P. T. A. Galek, P. McCabe, E. Pidcock, M. Platings, G. P. Shields, J. S. Stevens, M. Towler and P. A. Wood, *J. Appl. Cryst.*, 2020, **53**, 226–235.

[S6] G. Velde, F. M. Bickelhaupt, E. J. Baerends, C. F. Guerra, S. J. A. van Gisbergen, J. G. Snijders and T. Ziegler, *J. Comput. Chem.*, **2001**, *22*, 931–967.

[S7] ADF 2019.3, SCM, Theoretical Chemistry; Vrije Universiteit: Amsterdam, The Netherlands. Available online: https://www.scm.com/product/adf/.

[S8] S. Grimme, J. Antony, S. Ehrlich and H. Krieg, *J. Chem. Phys.*, **2010**, *132*, 154104.

[S9] L. Qu, H. Iguchi, S. Takaishi, F. Habib, C. F. Leong, D. M. D'Alessandro, T. Yoshida, H. Abe, E. Nishibori and M. Yamashita, *J. Am. Chem. Soc.*, **2019**, *141*, 6802–6806

[S10] S. Koyama, T. Tanabe, S. Takaishi, M. Yamashita and H. Iguchi, *Chem. Commun.*, **2020**, *56*, 13109–13112.

[S11] M. Cui, R. Murase, Y. Shen, T. Sato, S. Koyama, K. Uchida, T. Tanabe, S. Takaishi, M. Yamashita and H. Iguchi, *Chem. Sci.*, **2022**, *13*, 4902–4908.

[S12] S. S. Park, E. R. Hontz, L. Sun, C. H. Hendon, A. Walsh, T. V. Voorhis and M. Dincă, *J. Am. Chem. Soc.* **2015**, *137*, 1774–1777.

[S13] J. Y. Koo, Y. Yakiyama, G. R. Lee, J. Lee, H. C. Choi, Y. Morita and M. Kawano, *J. Am. Chem. Soc.* **2016**, *138*, 1776–1779.

[S14] D. Chen, H. Xing, Z. Sua and C. Wang, *Chem. Commun.,* **2016***, 52,* 2019–2022.

[S15] G. Skorupskii, K. N. Le, D. L. M. Cordova, L. Yang, T. Chen, C. H. Hendon, M. Q. Arguilla and M. Dincă, *Proc. Natl. Acad. Sci. U.S.A.* **2022**, *119,* e2205127119.